

RESEARCH ARTICLE | APRIL 15 2024

## Angle selectivity of liquid crystal superstructure and applications in bio-detection **FREE**

Ting-Hao Zhang (张廷颢) ; Bao-Fei Wan (万宝飞) ; Jun-Yang Sui (睦钧阳) ;  
Hai-Feng Zhang (章海锋)  



*Physics of Fluids* 36, 047123 (2024)

<https://doi.org/10.1063/5.0206791>

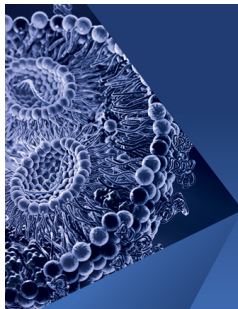


View  
Online



Export  
Citation

21 April 2024 10:08:19



## Physics of Fluids

Special Topic:

Flow and Lipid Nanoparticles

Guest Editors: Richard Braatz and Mona Kanso

**Submit Today!**

# Angle selectivity of liquid crystal superstructure and applications in bio-detection

Cite as: Phys. Fluids **36**, 047123 (2024); doi: [10.1063/5.0206791](https://doi.org/10.1063/5.0206791)

Submitted: 4 March 2024 · Accepted: 29 March 2024 ·

Published Online: 15 April 2024



View Online



Export Citation



CrossMark

Ting-Hao Zhang (张廷灏),  Bao-Fei Wan (万宝飞),  Jun-Yang Sui (睦钧阳),  and Hai-Feng Zhang (章海锋) 

## AFFILIATIONS

College of Electronic and Optical Engineering & College of Flexible Electronics (Future Technology), Nanjing University of Posts and Telecommunications, Nanjing 210023, China

<sup>a)</sup> Author to whom correspondence should be addressed: [hanlor@163.com](mailto:hanlor@163.com) and [hanlor@njupt.edu.cn](mailto:hanlor@njupt.edu.cn)

## ABSTRACT

In this paper, a temperature-controlled angle selection device based on a photonic bandgap is proposed, consisting of MLC-6608 liquid crystal (MLC) and common electrolytes stacked in layers. This device has an angular transmission stability for electromagnetic waves over a wide frequency band (600–660 THz). A high transmissivity ( $T > 0.85$ ) area, also called an angle window, is formed at 25° and 75°, and an area of zero transmissivity is formed beyond the angle window. The MLC is temperature-responsive, and the range of angle selection can be expanded or narrowed by temperature adjustment. When the MLC is replaced by the biological sample, it shows good sensing performance. It can be used to detect *in vitro* dermis, *in vivo* stratum corneum, and *in vivo* epidermis and it is of great significance in medicine, with a sensing sensitivity of 90.91°/refractive index unit.

Published under an exclusive license by AIP Publishing. <https://doi.org/10.1063/5.0206791>

## I. INTRODUCTION

Monochromatic plane electromagnetic waves (EWs) have three basic characteristics: frequency, propagation direction, and polarization, of which the study of frequency and polarization has been mature, but the control over the direction of propagation develops relatively slowly. Frequency selection becomes possible through optical fibers,<sup>1</sup> metamaterials,<sup>2</sup> waveguides,<sup>3</sup> photonic crystal (PC),<sup>4</sup> and plasmon.<sup>5</sup> The photonic bandgap (PBG)<sup>4,6,7</sup> of PC is used to achieve frequency selection through “band edge,”<sup>8</sup> to achieve polarization selection through the “embedded PC,”<sup>9</sup> gradient-index metasurface.<sup>10</sup> However, the research progress of angle selection is significantly behind the other two aspects. Directional selection of EWs has important applications in optical and thermal effects,<sup>11–13</sup> communication and information transmission,<sup>14</sup> lidar and sensors,<sup>15</sup> and laser processing and manufacturing.<sup>16</sup> The technology of using PC grating, diffraction effect, and Brewster angle<sup>17–19</sup> design devices with angle selectivity (AS) has been researched for some time, but it is still limited by narrow-band selectivity or depends on polarization mode, which greatly limits the deeper study of the angle selection structure.

In 2014, Shen *et al.*<sup>17,20</sup> pioneered the use of hierarchical mechanism and Brewster angle mode<sup>17,20</sup> to design a broadband anti-reflection structure for transverse magnetic (TM) waves, but the given structure did not have AS for transverse electric (TE) waves. In 2016, Iizuka *et al.*<sup>21</sup> proposed a polarization-independent anti-reflection

structure using the diffraction effect of PC, which was experimentally verified two years later. However, due to the frequency characteristics of PC, the proposed structure covers a very limited frequency range. In 2018, Qu *et al.*<sup>22</sup> designed a system that realized the function of broadband angle filters without relying on the polarization mode, but its rectangular coefficient was slightly lower and the frequency selection effect was average. In 2022, Wan *et al.*<sup>23,24</sup> achieved both broadband AS and polarization insensitivity, but it relies on superconducting materials, has an extremely high-temperature requirement, and is too difficult to achieve. For application potentials, it is a tall order to explore a balance between angle selection performance and bandwidth. To solve the above problems, liquid crystal (LC)<sup>25–27</sup> is added to the structure to improve the performance. The optical devices designed in the past that rely on LC have low transmissivity and poor AS, which are optimized in this paper. The MLC-6608 (MLC) used is a nematic LC. The refractive index of LC is mainly determined by temperature and wavelength.<sup>28</sup> When the wavelength and orientation of incident EWs are determined, the LC refractive index is mainly regulated by the temperature. The refractive index of the LC decreases with increasing temperature.

It has been the subject of widespread interest to detect the presence and concentration of human cells.<sup>29</sup> The conventional detection techniques are time-consuming, low precision, and large size.<sup>30</sup> Highly sensitive sensors with small size and instant response are

indispensable. The detection of human tissue cells is of positive significance for monitoring human health, disease prevention, and diagnosis. The design of sensors utilizing PC has been a topic of wide interest in recent years. Existing PC sensing techniques are mainly realized using defect modes,<sup>31</sup> tamm states,<sup>32</sup> and spin hall effects.<sup>33</sup> These sensing modes are based on wavelength modulation, and the dispersion effect cannot be ignored in the high-precision design requirements. In 2023, Sui *et al.*<sup>33</sup> proposed a sensing method by spin hall shift and applied it to bio-detection, but changes in the peaks are difficult to observe. This causes the result to be that the sensitivity is not as high as it could be in theory. Angle-selective sensors are based on angle modulation and utilize a sudden change in energy from 0 to 1 for sensing. This sensing method eliminates the effects caused by dispersion, and at the same time, features easy observation and strong resolution.

In this paper, by using the PBG structure of PC, a LC angle selection device (LCASD) that can work in the visible light band is designed. This device can realize stable angle selection over a 60 terahertz (THz) bandwidth, which is from 600 to 660 THz. The MLC in this design operates at room temperature ( $T_0 = 298$  K), and when the temperature changes, the refractive index property of the MLC also changes. When the LC layer is replaced with a biological solution, bio-detection can be realized. Measurements of *in vitro* dermis, *in vivo* stratum corneum, and *in vivo* epidermis were achieved with a sensitivity of  $90.91^\circ/\text{RIU}$ . The device is of great importance for medical clinical diagnosis and treatment.

## II. MODEL AND METHODS

LCASD, which realizes wide bandwidth angle selection, the structure, is shown in Fig. 1, the propagation direction of the wave vector is limited to the  $yo$ z plane. The structure is composed of layers of alternately arranged bismuth germanium oxide (BGO)<sup>34</sup> and MLC, which has a high performance of AS. The angle-transmissivity dependence is solved by using the transfer matrix method. In the model, BGO and MLC are alternately arranged, and the period  $N$  is 26. When the BGO operates in the frequency band in this paper, the refractive index is 2.67.<sup>34</sup> The thickness of BGO is  $d_1 = 166$  nm in the host structure and  $d_1/2 = 83$  nm in either side, and the thickness of MLC is  $d_3 = 72$  nm in the host structure and  $d_2 = 68$  nm in the structure on either side of the outside of the host structure (auxiliary structure).

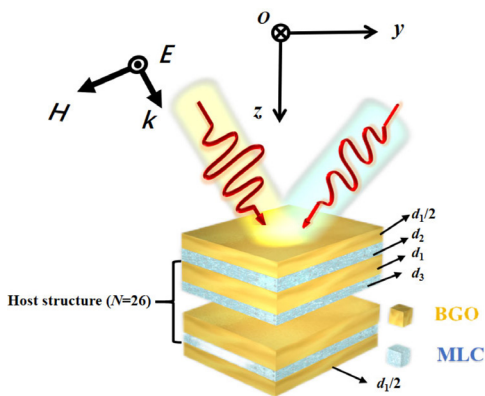


FIG. 1. The constructed LCASD model, which contains the host structure and the auxiliary structure, with BGO and MLC arranged alternately.

The mainstream method of calculating the LC refractive index is using the Cauchy extension equation<sup>24</sup> to calculate the temperature of the LC refractive index and wavelength general expression. In this way, it can be measured that the LC refractive index is  $n_e = 1.5655$ ,  $n_o = 1.4819$  when  $T_0 = 298$  K and they are all temperature-regulated. In this paper, the coordination of LC is mainly accomplished by the plane orientation of self-assembled nonionic amphiphiles guided by the electric field.<sup>35</sup> This method, proposed by Kim and Lee<sup>35</sup> in 2020, has the advantages of stable coordination and a simple method. The refractive index properties of LC are determined by the refractive index ellipsoid of the LC. When the EWs are incident in the TE mode, it corresponds to the ordinary light (o-light) of the LC.<sup>36</sup> This property is reflected in the simulation as the refractive index of the LC is not in the TE wave. In this paper, the distribution of the LC is determined by the analysis of the relationship between the incident light wavelength and the transmissivity. For the MLC materials, to calculate the refractive index of MLC at various wavelengths, the Cauchy extended model was introduced for fitting. According to the experimental results of Li *et al.*,<sup>28</sup> it can be seen that the expression of the long-axis refractive index and short-axis refractive index in the Cauchy extended model of LC is as follows:<sup>28</sup>

$$\begin{aligned} n_e &= A_e + \frac{B_e}{\lambda^2} + \frac{C_e}{\lambda^3}, \\ n_o &= A_o + \frac{B_o}{\lambda^2} + \frac{C_o}{\lambda^3}. \end{aligned} \tag{1}$$

When  $T_0 = 298$  K,  $A_e = 1.5359$ ,  $B_e = 0.0070$ ,  $C_e = 4.02 \times 10^{-17}$ ,  $A_o = 1.4609$ ,  $B_o = 0.0050$ , and  $C_o = 3.29 \times 10^{-17}$ . The angle selection band is 600 – 660 THz, and the effect of LC dispersion has been considered. The parameters of the MLC used in this paper are derived from experimental measurements, and the values of  $n_e$  and  $n_o$  are controlled by temperature, and the values of the refractive index corresponding to specific temperatures are given in Table I.<sup>24</sup>

The transfer matrix between the BGO and the MLC is given by the following formula, and the feature matrix of the single dielectric layer is listed here first:<sup>37</sup>

$$M = \begin{bmatrix} \cos \delta_i & -\frac{i}{\eta_i} \sin \delta_i \\ -i\eta_i \sin \delta_i & \cos \delta_i \end{bmatrix}. \tag{2}$$

TABLE I. Values of  $n_e$  and  $n_o$  for MLC at different temperatures and wavelengths.<sup>28</sup>

$T_0$ (K)	$\lambda$ (nm)					
	450		486		546	
	$n_e$	$n_o$	$n_e$	$n_o$	$n_e$	$n_o$
288	1.5766	1.4887	1.5717	1.4852	1.5654	1.4808
293	1.5733	1.4859	1.5687	1.4828	1.5622	1.4789
298	1.5704	1.4854	1.5655	1.4819	1.5595	1.4775
303	1.5678	1.4826	1.5628	1.4794	1.5564	1.4754
308	1.5645	1.4823	1.5598	1.4787	1.5534	1.4742
313	1.5612	1.4782	1.5558	1.4753	1.5500	1.4718
318	1.5577	1.4783	1.5530	1.4749	1.5467	1.4707
323	1.5543	1.4755	1.5494	1.4725	1.5432	1.4688

In Eq. (2),  $\eta_i$  and  $\delta_i$  are described as  $\eta_i = \sqrt{\epsilon_0/\mu_0} \times n_i \times \cos(\theta_i)$  and  $\delta_i = \frac{\omega}{c} \times d_i \times n_i \times \cos \theta$ , where  $\omega = 2\pi f$ ,  $\theta_i$  represents the propagation angle in  $i$ th layer and  $c$  represents the EWs velocity in a vacuum. For the case of a one-dimensional periodic structure, the characteristic matrix of a single medium layer can be applied layer by layer, for the first layer medium, the field vector at the left interface is  $E_N, H_N$ , the field vector of the right interface is  $E_{N+1}, H_{N+1}$ , and then, they have<sup>37</sup>

$$\begin{bmatrix} E_N \\ H_N \end{bmatrix} = (\mathbf{M}_N) \begin{bmatrix} E_{N+1} \\ H_{N+1} \end{bmatrix}. \quad (3)$$

By layers and by on, the one-dimensional periodic structure is shown in model Fig. 1

$$\begin{aligned} \begin{bmatrix} E_N \\ H_N \end{bmatrix} &= \Pi \mathbf{M}_i \begin{bmatrix} E_{N+1} \\ H_{N+1} \end{bmatrix} \\ &= (\mathbf{M}_{BGO} \mathbf{M}_{MLC}) (\mathbf{M}_{BGO} \mathbf{M}_{MLC})^N \mathbf{M}_{BGO} \begin{bmatrix} E_{N+1} \\ H_{N+1} \end{bmatrix}, \\ \mathbf{M} \begin{bmatrix} E_{N+1} \\ H_{N+1} \end{bmatrix} &= \begin{bmatrix} A & B \\ C & D \end{bmatrix} \begin{bmatrix} E_{N+1} \\ H_{N+1} \end{bmatrix}. \end{aligned} \quad (4)$$

The style  $(\mathbf{M}_{BGO} \mathbf{M}_{MLC}) (\mathbf{M}_{BGO} \mathbf{M}_{MLC})^N \mathbf{M}_{BGO}$  is a one-dimensional periodic structure characteristic matrix of the whole structure, where  $N = 26$ . The electromagnetic field component equations are listed on the first interface and  $N + 1$  interface, respectively, and the obtained  $E_1, H_1, E_{N+1}, H_{N+1}$  are substituted. The reflection coefficient  $r$  and transmission coefficient  $t$  can be written as, and the reflectance  $R$  and transmittance  $T$  can be expressed as follows:<sup>37</sup>

$$r = \frac{E_{r1}}{E_{i1}} = \frac{A\eta_0 + B\eta_0\eta_{N+1} - C - D\eta_{N+1}}{A\eta_0 + B\eta_0\eta_{N+1} + C + D\eta_{N+1}}, \quad (5)$$

$$t = \frac{E_{tN+1}}{E_{i1}} = \frac{2\eta_0}{A\eta_0 + B\eta_0\eta_{N+1} + C + D\eta_{N+1}}. \quad (6)$$

The reflectance  $R$  and transmittance  $T$  can be expressed as follows:

$$\begin{aligned} R &= |r|^2, \\ T &= |t|^2. \end{aligned} \quad (7)$$

Since the LCASD model shown in Fig. 1 uses air as the background, it can be described as  $\eta_0 = \eta_{N+1}$ ; thus, the transmissivity and other numerical values of the LCASD model can be calculated.

It is decided by Bloch's theorem that the field vector at the interface satisfies:<sup>37</sup>

$$\begin{bmatrix} E_{N+2} \\ H_{N+2} \end{bmatrix} = e^{ikd} \begin{bmatrix} E_N \\ H_N \end{bmatrix} \quad (k \text{ stands for Bloch wavevector}). \quad (8)$$

It can be obtained by the transfer matrix method:<sup>37</sup>

$$\begin{bmatrix} E_N \\ H_N \end{bmatrix} = (\mathbf{M}_{BGO} \mathbf{M}_{MLC}) \begin{bmatrix} E_{N+2} \\ H_{N+2} \end{bmatrix} = e^{ikd} \begin{bmatrix} E_{N+2} \\ H_{N+2} \end{bmatrix}. \quad (9)$$

By the definite solution condition  $[\det(\mathbf{M} - e^{ikd}) = 0]$ , the dispersion relation of the one-dimensional periodic structure in Fig. 1 can be obtained as follows.  $\eta_a$  and  $\eta_b$  correspond to the effective optical conductance of the two materials, and  $\delta_a$  and  $\delta_b$  correspond to the phase difference of the EWs passing through the interfaces<sup>38</sup>

$$\cos kd = \cos \delta_a \cos \delta_b - \frac{1}{2} \left( \frac{\eta_a}{\eta_b} + \frac{\eta_b}{\eta_a} \right) \sin \delta_a \sin \delta_b. \quad (10)$$

The formation of LCASD is based on the AS of the PBG, which can be explained by dispersion theory. Based on the dispersive nature of the PBG, when  $kd = 0$  or an integer multiple of  $\pi$ , corresponding to the PBG, the incident light is completely reflected.<sup>37</sup> As shown in Fig. 2(a), when the angle of the incident light increases, the bandgap moves in the direction of high frequency. The white dashed line is the contour line for  $T = 0.85$ . Therefore, the corresponding angle window (AW) will also be formed at  $25^\circ$  and  $75^\circ$ . The dispersion distribution in the selected frequency band range is drawn, clearly shown in Fig. 2(b), and the purple dashed line is the contour line for  $T = 0.85$ . When the EWs enter the TE wave, in the meantime, the angle of incidence increases from  $0^\circ$ , and the structure maintains high transmissivity within a certain angle. In the selected frequency band range, the

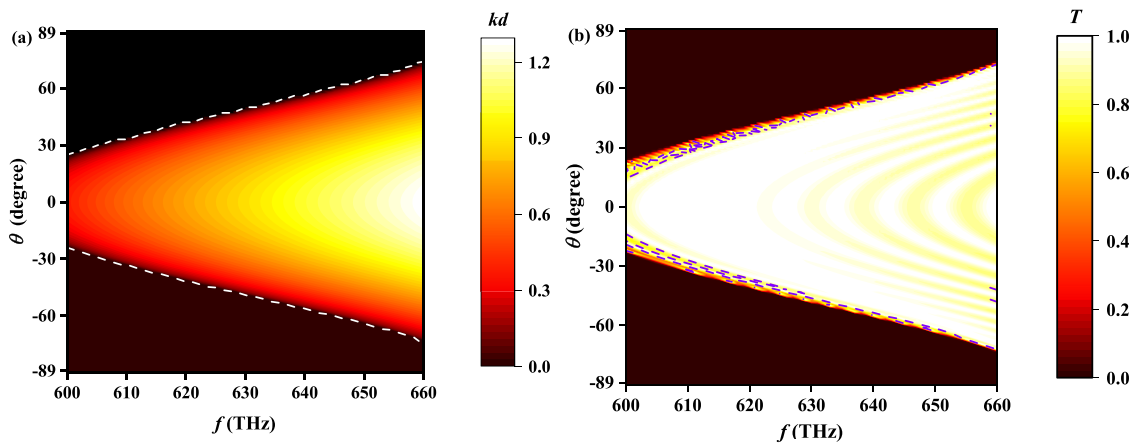


FIG. 2. (a) Dispersion distribution of LCASD and (b) schematic representation of the AS of the structure.

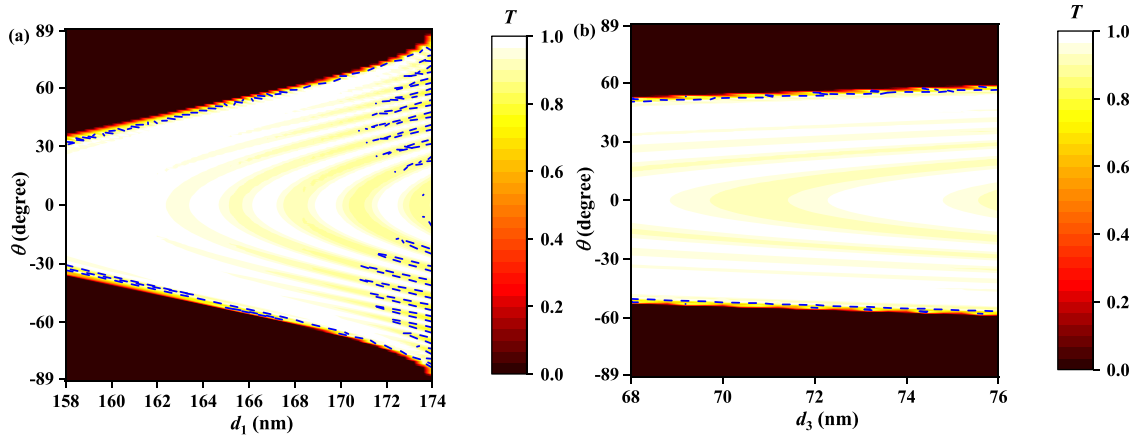


FIG. 3. Parameter discussion on thickness design of LCASD; (a)  $d_1$  and (b)  $d_3$ .

structure has good selectivity for electromagnetic waves incident from  $25^\circ$  to  $75^\circ$ .

### III. ANALYSIS AND DISCUSSION

The LCASD, AW, and transmissivity stability are important indicators of properties. Exceeding the range will lead to several indicators such as fit and sensitivity, so the AW has a corresponding design requirement. The point of  $f = 640$  THz is chosen for the discussion of the tunable nature of the AW as well as the parameters discussion. In the TE wave, the thickness of BGO in each layer of the host structure will affect the performance of LCASD. As shown in Fig. 3(a), the blue dashed line represents  $T = 0.85$ . AW becomes larger as the thickness of this layer structure becomes larger, when the thickness of this layer exceeds 170 nm, and the transmission stability is greatly reduced. The dispersive nature of the PBG shows that AW decreases when frequency decreases. Within the selected frequency band range, the variation of AW with frequency occurs from  $25^\circ$  to  $75^\circ$ . When  $f = 640$  THz, the corresponding AW is  $60^\circ$  and  $d_1 = 166$  nm meets this need. Considering the errors in thickness in actual manufacturing, the effects

of different thicknesses are discussed in Fig. 3(b). The thickness of this layer of medium in this paper is 72 nm, and the blue dashed line indicates  $T = 0.85$ . When the thickness changes by  $\pm 4$  nm, the AW changes are minimal, indicating that the design can withstand the small thickness error of the LC.

The effects of the refractive index change of the host structure are discussed on the angle selection performance of LCASD in Fig. 4. An isotropic dielectric BGO with a refractive index of 2.67 (Ref. 34) is used in the LCASD considering the effect of spectral redshift on the AW range and transmittance stability. The blue dashed line indicates  $T = 0.85$ , and as in Fig. 3(a), the refractive index of the design needs to satisfy an AW of  $60^\circ$  at this frequency point. In Fig. 4, when EWs are incident under the TE wave, AW becomes larger with increasing refractive index. When the refractive index increases, the stability of the transmittance of the LCASD decreases, the blue dashed line in Fig. 4 becomes smooth, and it collapses when the refractive index

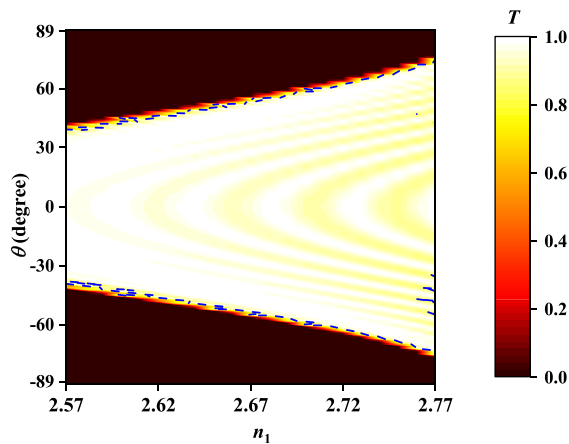


FIG. 4. Effects of the refractive index change of the medium in the main structure on the performance of LCASD.

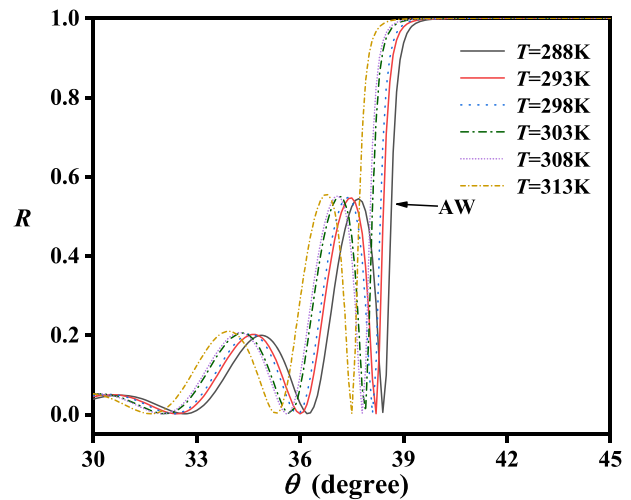


FIG. 5. When the temperature changes, the LC is modulated and the AW of the LCASD changes.

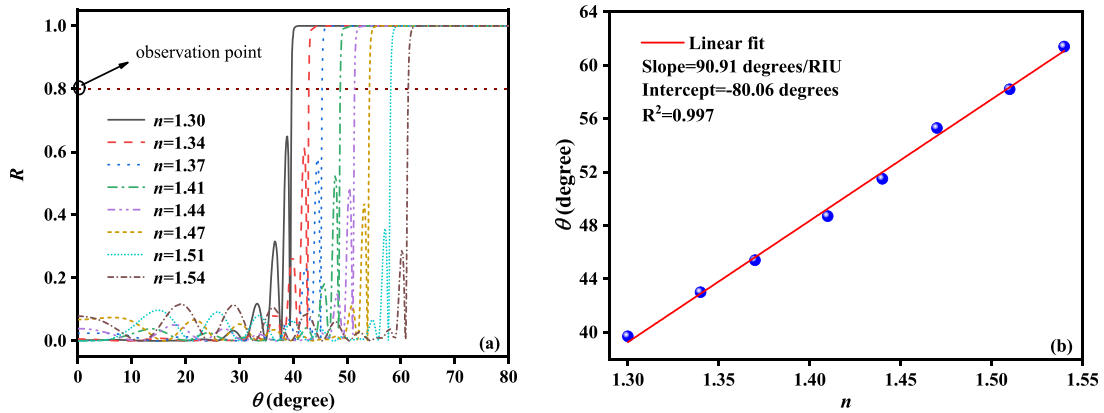


FIG. 6. (a) Spectral analysis with a refractive index between 1.30 and 1.54 and (b) linear fitting results when detecting in refractive index change.

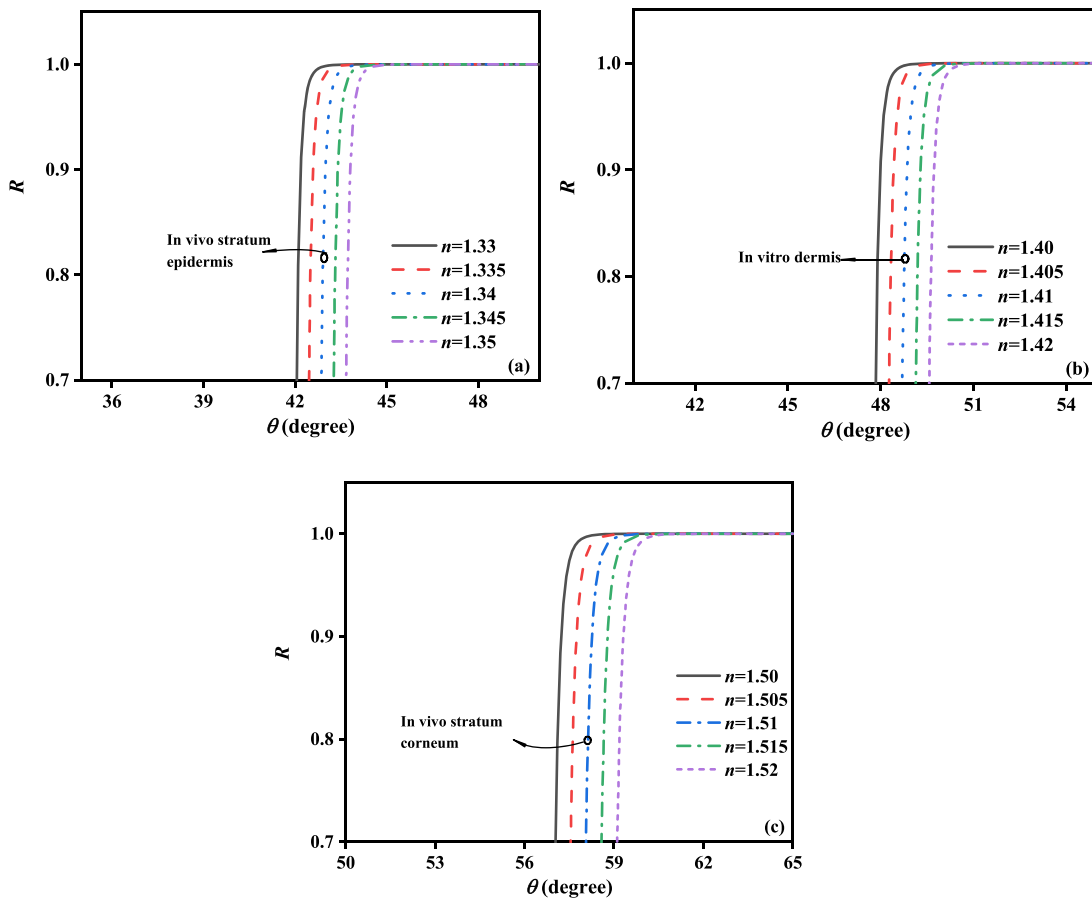


FIG. 7. Error analysis of three human tissue cell sensing; (a) *in vivo* epidermis; (b) *in vitro* dermis; and (c) *in vivo* stratum corneum.

increases. BGO with a refractive index of 2.67 exists in a stable form and combines transmissivity stabilization and AS.

When the temperature changes, the  $n_o$  of the LC changes accordingly, resulting in the movement of the AW, creating the

function of a tunable AW. In Fig. 5, for EWs incident in the TE wave, the range of AW is changed when the temperature is changed. A temperature change of 30 K can be the range of AW shifted by nearly  $2^\circ$ , creating a tunable effect. It can be seen that the temperature has a

certain regulating effect in the TE wave and provides tunable effects for the device.

AW formed by PBG is a new type of sensing.<sup>38</sup> The conventional PC sensing is usually realized using peak size changes or displacements, which are not very observable and may be interfered with by harmonics. Angle-selective sensors utilize a point where the reflectivity jumps from 1 to 0 for sensing. Conventional PC sensors generally set the location of a substance in the structure as a cavity. However, the embedding and removing of solid substances is cumbersome. In this paper, the internal structure of the sensor contains LC, which is in the flow state. In the application, it is only necessary to pour the LC out of the device and introduce the tissue fluid to be measured into the device to realize the sensing instantly. A variety of tissue cells are present in the human body, of which *in vitro* dermis, *in vivo* stratum corneum, and *in vivo* epidermis<sup>29</sup> are important indicators for monitoring human health and clinical procedures. The point with a reflectance of 0.8 is selected as the observation point. As shown in Fig. 6(a), the angle at which the reflectivity undergoes a jump when the LC layer is replaced with a cavity varies linearly. The fitted curve is given in Fig. 6(b), and the sensitivity reaches  $90.91^\circ/\text{RIU}$ , and  $R^2$  values exceed 0.997, which meets the performance requirements of bio-detection. In 2023, Wan *et al.*<sup>38</sup> proposed an angle-selective sensor by utilizing the dielectric properties of epsilon-negative materials, and its maximum sensitivity is  $-57.1^\circ/\text{RIU}$ . The sensor proposed in this paper has higher sensitivity, which helps to obtain better bio-detection performance.

Tearney *et al.*<sup>29</sup> used optical coherence tomography to determine the refractive index of tissue cells. Under this method, the maximum error of determination was 0.03 for *in vitro* dermis, 0.02 for *in vivo* stratum corneum, and 0.01 for *in vivo* epidermis. The angle deviations when the refractive indices corresponding to the three types of human histiocytes were in error are given in Figs. 7(a)–7(c). When the refractive index error is set to 0.05, the angle of determination was shifted by  $0.4^\circ$  for *in vitro* dermis,  $0.4^\circ$  for *in vivo* stratum corneum, and  $0.5^\circ$  for *in vivo* epidermis.

#### IV. CONCLUSION

In conclusion, a function of EWs direction control in space is realized through a cascade of LCASD. The function of AS in the visible light band and bio-detection is realized in this paper. The direction of the EWs can be realized by the PBG and be regulated by the incident angle of PC, layered stack BGO and LC materials. The AW can be regulated by temperature. The LCASD operates in the visible wavelength range, and this modulation can be utilized for visual effects. The measurements of the *in vitro* dermis, *in vivo* stratum corneum, and *in vivo* epidermis are realized. The modulating effect of temperature on LC has the potential effect of extending the sensing range,<sup>34</sup> offering the method to measure more biological solutions. This device realizes angle selection with 60 THz bandwidth in the visible wavelength band and introduces LC to make AW temperature adjustable. Three types of tissue cell measurements are performed simultaneously, providing a fast and effective new way for human health monitoring.

#### ACKNOWLEDGMENTS

This work was supported by the Postgraduate Research & Practice Innovation Program of Jiangsu Province (Grant No. KYCX23\_1004).

#### AUTHOR DECLARATIONS

##### Conflict of Interest

The authors have no conflicts to disclose.

##### Author Contributions

**Ting-Hao Zhang:** Investigation (lead); Validation (lead); Writing – original draft (lead). **Bao-Fei Wan:** Formal analysis (lead); Funding acquisition (lead); Visualization (lead). **Jun-Yang Sui:** Conceptualization (supporting); Data curation (lead); Formal analysis (equal); Validation (lead). **Hai-Feng Zhang:** Conceptualization (lead); Project administration (lead); Supervision (lead); Writing – review & editing (lead).

##### DATA AVAILABILITY

The data that support the findings of this study are available from the corresponding author upon reasonable request.

##### REFERENCES

- N. Hayashi, Y. Mizuno, D. Koyama, and K. Nakamura, “Marked enhancement in the efficiency of deep-ultraviolet AlGaIn light-emitting diodes by using a multiquantum-barrier electron blocking layer,” *Appl. Phys. Express* **3**, 31002–31002 (2010).
- B. X. Wang, G. Duan, W. Lv, Y. Tao, H. Xiong, D. Q. Zhang, G. Yan, and F. Z. Shu, “Design and experimental realization of triple-band electromagnetically induced transparency terahertz metamaterials employing two big-bright modes for sensing applications,” *Nanoscale* **15**, 18435–18446 (2023).
- A. Fiore, V. Berger, E. Rosencher, P. Bravetti, N. Laurent, and J. Nagle, “Phase-matched mid-infrared difference frequency generation in GaAs-based waveguides,” *Appl. Phys. Lett.* **71**, 3622–3624 (1997).
- R. E. Hamam, I. Celanovic, and M. Soljacic, “Angular photonic band gap,” *Phys. Rev. A* **83**, 035806 (2011).
- Y. Hwang, J. Shin, J. E. Kim, H. Y. Park, and C. S. Kee, “Frequency selective heterojunction metal-insulator-metal mirror for surface plasmons,” *Phys. Rev. B* **83**, 235131 (2011).
- E. Yablonovitch, “Photonic band-gap structures,” *J. Opt. Soc. Am. B* **10**, 283–295 (1993).
- J. D. Joannopoulos, S. G. Johnson, J. N. Winn, and R. D. Meade, *Photonic Crystals: Molding the Flow of Light*, 2nd ed. (Princeton University Press, 2008).
- G. A. Turnbull, P. Andrew, M. J. Jory, W. L. Barnes, and I. D. W. Samuel, “Relationship between photonic band structure and emission characteristics of a polymer distributed feedback laser,” *Phys. Rev. B* **64**, 125122 (2001).
- E. Matioli, S. Brinkley, K. M. Kelchner, S. Nakamura, S. DenBaars, J. Speck, and C. Weisbuch, “Polarized light extraction in m-plane GaN light-emitting diodes by embedded photonic-crystals,” *Appl. Phys. Lett.* **98**, 251112 (2011).
- Q. Yang, H. Xiong, J. H. Deng, B. X. Wang, W. X. Peng, and H. Q. Zhang, “Polarization-insensitive composite gradient-index metasurface array for microwave power reception,” *Appl. Phys. Lett.* **122**, 253901 (2023).
- B. E. Nelson, M. Gerken, D. A. B. Miller, R. Piestun, C. C. Lin, and J. S. Harris, “Use of a dielectric stack as a one-dimensional photonic crystal for wavelength demultiplexing by beam shifting,” *Opt. Lett.* **25**, 1502–1504 (2000).
- R. Ozaki, T. Matsui, M. Ozaki, and K. Yoshino, “Electrically color-tunable defect mode lasing in one-dimensional photonic-band-gap system containing liquid crystal,” *Appl. Phys. Lett.* **82**, 3593–3595 (2003).
- B. K. Singh and P. C. Pandey, “Effect of temperature on terahertz photonic and omnidirectional band gaps in one-dimensional quasi-periodic photonic crystals composed of semiconductor InSb,” *Appl. Opt.* **55**, 5684–5692 (2016).
- C. Niclass, M. Soga, H. Matsubara, S. Kato, and M. Kagami, “A 100-m range 10-Frame/s 340 × 96-pixel time-of-flight depth sensor in 0.18- $\mu\text{m}$  CMOS,” *IEEE J. Solid-State Circuits* **48**, 559 (2013).
- T. Komine and M. Nakagawa, “Fundamental analysis for visible-light communication system using LED lights,” *IEEE Trans. Consum. Electron.* **50**, 100 (2004).

- <sup>16</sup>B. J. Lee, C. J. Fu, and Z. M. Zhang, “Coherent thermal emission from one-dimensional photonic crystals,” *Appl. Phys. Lett.* **87**, 071904 (2005).
- <sup>17</sup>Y. C. Shen, D. X. Ye, C. I. J. SG, J. D. Joannopoulos, and M. Soljačić, “Optical broadband angular selectivity,” *Science* **343**, 1499–1501 (2014).
- <sup>18</sup>Y. C. Shen, D. X. Ye, L. Wang, I. Celanovic, L. X. Ran, J. D. Joannopoulos, and M. Soljačić, “Metamaterial broadband angular selectivity,” *Phys. Rev. B* **90**, 125422 (2014).
- <sup>19</sup>C. Argyropoulos, K. Q. Le, N. Mattiucci, G. D’Aguanno, and A. Alù, “Broadband absorbers and selective emitters based on plasmonic Brewster metasurfaces,” *Phys. Rev. B* **87**, 205112 (2013).
- <sup>20</sup>Y. C. Shen, C. W. Hsu, Y. X. Yeng, J. D. Joannopoulos, and M. Soljačić, “Broadband angular selectivity of light at the nanoscale: Progress, applications, and outlook,” *Appl. Phys. Rev.* **3**, 011103 (2016).
- <sup>21</sup>H. Iizuka, N. Engheta, and S. Sugiura, “Extremely small wavevector regime in a one-dimensional photonic crystal heterostructure for angular transmission filtering,” *Opt. Lett.* **41**, 3829–3832 (2016).
- <sup>22</sup>Y. R. Qu, Y. C. Shen, K. Z. Yin, Y. Q. Yang, Q. Li, M. Qiu, and M. Soljačić, “Polarization-independent optical broadband angular selectivity,” *ACS Photonics* **5**, 4125–4131 (2018).
- <sup>23</sup>B. F. Wan, H. F. Zhang, and P. X. Wang, “Nonreciprocal absorber with a narrow band of angular polarization sensitive regions based on a quasi-periodic structure,” *Opt. Lett.* **46**, 1934–1937 (2021).
- <sup>24</sup>B. F. Wan, H. N. Ye, and H. F. Zhang, “Ultra-wideband polarization insensitive angle filter based on ENZ characteristics and dynamic antireflection structures,” *Photonics* **9**, 854 (2022).
- <sup>25</sup>T. D. Ibragimov and G. M. Bayramov, “Novel type of tunable infrared filters based on the Al<sub>2</sub>O<sub>3</sub> particles—Liquid crystal system,” *Infrared Phys. Technol.* **55**, 56–59 (2012).
- <sup>26</sup>S. Hayashi and T. Okamoto, “Plasmonics: Visit the past to know the future,” *J. Phys. D: Appl. Phys.* **45**, 433001 (2012).
- <sup>27</sup>T. Baba, N. Fukaya, and J. Yonekura, “Observation of light propagation in photonic crystal optical waveguides with bends,” *Electron. Lett.* **35**, 654 (1999).
- <sup>28</sup>J. Li, C. H. Wen, S. Gauza, R. Lu, and S. T. Wu, “Refractive indices of liquid crystals for display applications,” *J. Disp. Technol.* **1**, 51–61 (2005).
- <sup>29</sup>G. J. Tearney, M. E. Brezinski, J. F. Southern, B. E. Bouma, M. R. Hee, and J. G. Fujimoto, “Determination of the refractive index of highly scattering human tissue by optical coherence tomography,” *Opt. Lett.* **20**, 2258–2260 (1995).
- <sup>30</sup>L. Zeng, L. Wang, and J. Hu, “Current and emerging technologies for rapid detection of pathogens,” *Biosens. Technol. Detect. Pathog.* **73178**, 6–19 (2018).
- <sup>31</sup>B. F. Wan, Y. Xu, Z. W. Zhou, D. Zhang, and H. F. Zhang, “Theoretical investigation of a sensor based on one-dimensional photonic crystals to measure four physical quantities,” *IEEE Sens. J.* **21**(3), 2846–2853 (2021).
- <sup>32</sup>B. F. Wan, Q. Y. Wang, H. M. Peng, H. N. Ye, and H. F. Zhang, “A late-model optical biochemical sensor based on OTS for methane gas and glucose solution concentration detection,” *IEEE Sens. J.* **21**, 21465–21472 (2021).
- <sup>33</sup>J. Y. Sui, J. H. Zou, S. Y. Liao, B. X. Li, and H. F. Zhang, “High sensitivity multi-scale and multitasking terahertz Janus sensor based on photonic spin Hall effect,” *Appl. Phys. Lett.* **122**, 231105 (2023).
- <sup>34</sup>M. Simon, F. Mersch, C. Kuper, S. Mendricks, S. Wevering, J. Imbrock, and E. Kraetzig, “Refractive indices of photorefractive bismuth titanate, barium-calcium titanate, bismuth germanium oxide, and lead germanate,” *Phys. Status Solidi A* **159**, 559 (1997).
- <sup>35</sup>J. Kim and J. H. Lee, “A new approach for directional homogeneous alignment of liquid crystals using electric field-guided orientation of nonionic amphiphiles,” *J. Mol. Liq.* **319**, 114187 (2020).
- <sup>36</sup>Y. Ohno, T. Ishinabe, T. Miyashita, and T. Uchida, “Highly accurate method for measuring ordinary and extraordinary refractive indices of liquid crystal materials, cell thickness, and pretilt angle of liquid crystal cells using ellipsometry,” *Jpn. J. Appl. Phys., Part 1* **48**, 051502 (2009).
- <sup>37</sup>L. M. Qi, Z. Q. Yang, F. Lan, X. Gao, and Z. J. Shi, “Properties of obliquely incident electromagnetic wave in one-dimensional magnetized plasma photonic crystals,” *Phys. Plasmas* **17**, 042501 (2010).
- <sup>38</sup>B. F. Wan, H. N. Ye, D. Zhang, and H. F. Zhang, “A variable refractive index sensor based on epsilon-near-zero spatial selection structure and its potential in biological detection,” *New J. Phys.* **25**, 023003 (2023).